SAND74-0433

Unlimited Release

Acoustic Radiation From Cylindrical Bodies

When printing a copy of any digitized SAND Report, you are required to update the markings to current standards.

W. N. Sullivan, J. F. Banas

Prepared by Sandia Laboratories, Albuquerque, New Mexico 87115 and Livermore, California 94550 for the United States Energy Research and Development Administration under Contract AT(29-1)-789

Printed May 1975

Sandia Laboratories

SF 2900 Q(7-73)

Issued by Sandia Laboratories, operated for the United States Energy Research and Development Administration by Sandia Corporation.

NOTICE

This report was prepared as an account of work sponsored by the United States Government. Neither the United States nor the United States Energy Research and Development Administration, nor any of their employees, nor any of their contractors, subcontractors, or their employees, makes any warranty, express or implied, or assumes any legal liability or responsibility for the accuracy, completeness or usefulness of any information, apparatus, product or process disclosed, or represents that its use would not infringe privately owned rights.

SAND74-0433
Unlimited Release
Printed May 1975

ACOUSTIC RADIATION FROM CYLINDRICAL BODIES

W. N. Sullivan
Applied Mechanics Division III, 1544

J. F. Banas
Systems Studies Division IV, 4734

Sandia Laboratories, Albuquerque, NM 87115

ABSTRACT

Two codes have been written to generate surface and field pressure distributions about finite length vibrating cylindrical bodies. The theoretical basis for the programs, the surface Helmholtz integral formulation of the acoustic radiation problem, is briefly described along with the details of the numercial methods used. The codes are verified by using a class of exact solutions, and sample results are given for the radiation pressures from a simple finite cylinder with rigid end caps.

TABLE OF CONTENTS

		Page
I.	INTRODUCTION	5
II.	THEORY	6
	Helmholtz Integral Formulation	6
	Solution Techniques	7
III.	NUMERICAL METHODS	9
	Source Geometry and Nomenclature	9
	Computation of the External Pressure Field	10
	Computation of the Impedance Matrix	12
IV.	COMPUTER CODE CHECKOUT	16
	Verification Method	16
	Computation Time and Error for RADIAT	16
	Computation Time and Error for IMPED	17
V.	ALTERNATIVE METHOD FOR COMPUTING IMPEDANCE MATRIX	19
VI.	RESULTS FOR THE CYLINDER WITH RIGID END CAPS	20
	Moderate Frequency (ka = 1; ka = 2)	20
	Very Low Frequency (ka = 0.025)	23
VII.	SUMMARY AND CONCLUSIONS	25
REFERENCES		27
APPENDIX A - INPUT/OUTPUT INFORMATION FOR RADIAT AND IMPED		29

ACOUSTIC RADIATION FROM CYLINDRICAL BODIES

I. INTRODUCTION

Use of cylindrical low-frequency acoustic sources at Sandia Laboratories has led to a number of questions regarding the nature of acoustic fields generated by such devices. Of particular interest to sonar applications is the far field radiation pattern characteristic of a source. Field patterns can be obtained experimentally for given operating conditions through acoustic field surveys. However, a lack of generality and considerable tedium is associated with this approach, especially since practical limitations necessitate use of a small number of hydrophones. These experimental difficulties provided the major motivation for pursuit of analytical solutions.

The surface Helmholtz integral formulation of the field equations is the basis for numerical solutions of the acoustic radiation problem for a surface whose normal velocity is specified. A method, described in detail by Schenck [1], has been developed and applied in recent years by several authors [2, 3, 4]. The radiation analysis consists of two basic parts. First, the surface pressure distribution corresponding to a prescribed surface velocity distribution is generated. Second, by using the surface pressure and velocity functions as boundary conditions, near and far field pressure distributions are determined.

Analyses presented here are for finite length cylindrical geometries with characteristic cylinder dimensions as parameters. More general, nonaxisymmetric geometries can be considered by similar methods, but with additional expense in complexity and computation time.

An incidental outcome from the solution is the so-called impedance matrix, characteristic of the system geometry and frequency. This matrix, once found, permits rapid generation of surface pressures resulting from an arbitrary distribution of velocities on the radiating body. These surface pressures can be readily coupled with numerical [5] or analytical structural solutions for study of vibrating elastic structures in acoustic media.

II. THEORY

Helmholtz Integral Formulation

Consider a closed surface which is harmonically vibrating and radiating sound to an unbounded acoustic medium. Pressure at a field point P, external to the surface S, is given by the Helmholtz integral formula [1]

$$p(P) = -\frac{i\rho\omega}{4\pi}\iint_S \frac{e^{ikD(P,s)}}{D(P,s)}\,u(s)\,dS + \frac{1}{4\pi}\iint_S p(s)\,\frac{\partial}{\partial n(s)}\left(\frac{e^{ikD(P,s)}}{D(P,s)}\right)dS \tag{1}$$

where $D(P,s)$ is distance between field point P and the surface point s at dS, $u(s)$ is a given normal velocity distribution, $p(s)$ is the pressure distribution, ρ is the density of the acoustic medium, ω is frequency and k is the wave number. The partial derivative is taken with respect to the outward normal to the surface at point s. The harmonic time dependence $e^{-i\omega t}$ has been suppressed for clarity.

The surface pressure distribution $p(s)$ is not arbitrary; rather, it must satisfy the integral Equation (1) resulting from letting $P \to s'$, some point on S.

$$p(s') = \frac{-i\rho\omega}{2\pi}\iint_S \frac{e^{ikD(s',s)}}{D(s',s)}\,u(s)\,dS + \frac{1}{2\pi}\iint_S p(s)\,\frac{\partial}{\partial n(s)}\left(\frac{e^{ikD(s',s)}}{D(s',s)}\right)dS\ . \tag{2}$$

The new factor $1/2\pi$ is introduced to account for discontinuities which occur in the integrals as $P \to s'$. These are improper integrals since D vanishes at $s = s'$. It is implicitly assumed in Equation (2) that principal values of the integrals be used.

Integral Equations (1) and (2) are the basic tools used here to determine the radiation fields about a body with a prescribed normal surface velocity distribution. Equation (2) is solved first to determine the surface pressure distribution. This distribution is then available for Equation (1) to calculate pressure at field points of interest.

Solution Techniques

Equation (2) is solved by reducing the integral equation to a discrete set of linear algebraic equations. Following the method suggested by Schenck [1] and described in [5], the body is assigned N nodes denoted by subscript j. Surface pressures and velocities are approximated by

$$p^*(s) \approx \sum_{j=1}^{N} \Psi_j(s) p^*_j$$

$$u(s) \approx \sum_{j=1}^{N} \Psi_j(s) u_j \tag{3}$$

where p^* is pressure normalized by $\rho\omega$. In Equation (3), p^*_j and u_j are nodal pressures and velocities, respectively, and Ψ_j are interpolation functions, usually taken to be linear. Note that $\Psi_j(s_k) = \delta_{jk}$, the Kronecker delta, where s_k are position coordinates of node k. Utilizing the above approximations in Equation (2) and generating N equations by satisfying Equation (2) at each point $s' = s_j$, it follows that

$$A\underline{p}^* = B\underline{u}$$

where $\underline{p}^*$ and $\underline{u}$ are vectors of the nodal pressures and velocities. The matrices A and B have elements given by

$$A_{j\ell} = \delta_{j\ell} - \frac{1}{2\pi} \iint_S \Psi_\ell(s) \frac{\partial}{\partial n(s)} \left(\frac{e^{ikD(s_j, s)}}{D(s_j, s)} \right) dS$$

and

$$B_{j\ell} = \frac{-i}{2\pi} \iint_S \Psi_\ell(s) \frac{e^{ikD(s_j, s)}}{D(s_j, s)} dS \ . \tag{4}$$

The impedance matrix Z is defined as $A^{-1}B$. Thus,†

$$\underline{p} = \rho\omega Z\underline{u} \ . \tag{5}$$

For a given geometry, Z is a function only of frequency. Once the matrix is found for a range of frequencies, surface pressure distributions can be rapidly determined by simple matrix multiplication.

---

†It has been shown [1] that the matrix A can be singular for certain frequencies. These characteristic frequencies are relatively high for the applications considered here and, therefore, methods for circumventing the problem will not be discussed.

Once the vector of nodal pressures is known, pressure at an external field point P is found by applying the approximations in Equation (3) to the Helmholtz integral Equation (1). Making this substitution yields a simple result for the field pressure $p^*(P)$,

$$p^*(P) = \sum_{j=1}^{N} (a_j p^*_j + b_j u_j) \tag{6}$$

where vectors $\underline{a}$ and $\underline{b}$ are given by

$$a_j = \frac{1}{4\pi} \iint_S \Psi_j(s) \frac{\partial}{\partial n(s)} \left(\frac{e^{ikD(P,s)}}{D(P,s)} \right) dS$$

and

$$b_j = \frac{-i}{4\pi} \iint_S \Psi_j(s) \frac{e^{ikD(P,s)}}{D(P,s)} dS \ . \tag{7}$$

Two computer codes, IMPED and RADIAT , have been written to effect the discrete integration of the impedance and radiation formulas, respectively. The programs in their present form are restricted to axially symmetric bodies made up of any connected combination of disc and cylindrical surfaces. Furthermore, the surface velocity distribution must be axisymmetric. Section III contains an outline of the numerical methods used and numerical results for a few selected problems. Appendix A contains a description of input/output information.

III. NUMERICAL METHODS

Source Geometry and Nomenclature

The class of geometries which will be considered consists of axisymmetric bodies made up of any connected combination of discs and cylinders. In general, a surface begins and ends with a disc, while the component surfaces alternate between disc and cylinder. An arbitrary number of nodes is assigned to each component surface. Each corner is assigned two nodes with the coordinates of the corner in order to avoid any ambiguity in the normal derivative. To familiarize the reader, Figure 1 presents an example consisting of seven component surfaces to which 27 nodes are assigned.

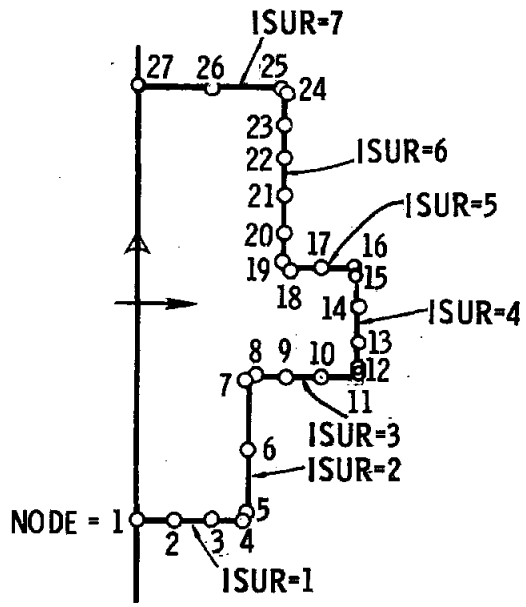

Figure 1. Example Source Geometry

Table I describes the relevant nomenclature together with values for the example of Figure 1.

TABLE I

Nomenclature for Surface

Parameter	Description	Value for Example		
N	Number of nodes	27		
NSUR	Number of component surfaces	7		
ISUR	Index of component surface (1 is always assigned to lowest disc)	1, 2, 3, 4, 5, 6, 7		
N_1(ISUR)/N_2(ISUR)	Node beginning/ending component surface ISUR	ISUR	N_1	N_2
		1	1	4
		2	5	7
		3	8	11
		4	12	15
		5	16	18
		6	19	24
		7	25	27
NCOR	Number of corners (always NSUR-1)	6		
ICOR(I)	First node of corner I	4, 7, 11, 15, 18, 24		
ZO	z coordinate value for Node 1	-6		
DRZ(ISUR)	Change in z or r coordinate for component surface ISUR (nodes for a given component surface are equally spaced)	+3, +4, +3, +3, -2, +5, -4		

A surface is completely specified by the following information:

N, NCOR, (ICOR(I), I=1, NCOR), ZO, (DRZ(ISUR), ISUR=1, NSUR)

Computation of the External Pressure Field

The integration of Equation (1) is relatively simple owing to the regularity of the integrands. A cylindrical coordinate system (r, θ, z) is used for points s on the surface of the body while a spherical coordinate system (R, ϕ, θ') is used for points P in the field. Because of the prescribed symmetry of the surface and surface velocity distribution, the nodal pressures and velocities are independent of θ. Also, θ' is taken to be zero without loss of generality. Utilizing the nomenclature of the previous section, Equation (1) is discretized to give

$$p^*(P) = \sum_{\substack{\text{ISUR}\\ \text{odd}}} \sum_{j=N_1}^{N_2-1} \left\{ \frac{-i}{4\pi} \int_{r_j}^{r_{j+1}} r\left[u_j + \frac{(u_{j+1} - u_j)}{(r_{j+1} - r_j)}(r - r_j)\right] \int_{-\pi}^{\pi} \frac{e^{ikD}}{D}\, d\theta dr \right.$$

$$\left. + \frac{1}{4\pi} \int_{r_j}^{r_{j+1}} r\left[p^*_j + \frac{(p^*_{j+1} - p^*_j)}{(r_{j+1} - r_j)}(r - r_j)\right] \int_{-\pi}^{\pi} \frac{\partial}{\partial z}\left(\frac{e^{ikD}}{D}\right) d\theta dr \right\}$$

$$+ \sum_{\substack{\text{ISUR}\\ \text{even}}} \sum_{j=N_1}^{N_2-1} \left\{ \frac{-ir}{4\pi} \int_{z_j}^{z_{j+1}} \left[u_j + \frac{(u_{j+1} - u_j)}{(z_{j+1} - z_j)}(z - z_j)\right] \int_{-\pi}^{\pi} \frac{e^{ikD}}{D}\, d\theta dz \right.$$

$$\left. + \frac{r}{4\pi} \int_{z_j}^{z_{j+1}} \left[p^*_j + \frac{(p^*_{j+1} - p^*_j)}{(z_{j+1} - z_j)}(z - z_j)\right] \int_{-\pi}^{\pi} \frac{\partial}{\partial r}\left(\frac{e^{ikD}}{D}\right) d\theta dz \right\} \tag{8}$$

where distance D between the surface point (r, θ, z) and the field point (R, ϕ) is given by

$$D = \left[(R \sin\phi - r \cos\theta)^2 + (r \sin\theta)^2 + (R \cos\phi - z)^2\right]^{1/2} .$$

On a disc (i.e., ISUR odd), z is constant; on a cylinder (i.e., ISUR even), r is constant. It should be noted that the only approximation contained in Equation (8) is the assumed linear interpolation formula based on nodal values of pressure and velocity.

The computer code RADIAT utilizes an adaptive 7-point Newton-Cotes algorithm to perform integration in θ. Integration in r and z is performed from user specification by either a trapezoidal rule algorithm with functional evaluations at the nodes or an adaptive Simpson's rule algorithm on each component surface. The Newton-Cotes algorithm and the Simpson's algorithm are QNC7 and QNC3, respectively, in the Sandia Mathematical Library [6]. Computational time and accuracy will be discussed in a subsequent section.

The so-called far field pressure pattern is obtained by neglecting terms in the near field solution Equation (8) which are of higher order than 1/R. Thus, the following limits are introduced

$$\frac{e^{ikD}}{D} \rightarrow \frac{e^{ik(R-r\cos\theta\sin\phi-z\cos\phi)}}{R}$$

$$\frac{\partial}{\partial z}\left(\frac{e^{ikD}}{D}\right) \rightarrow \frac{-ik\cos\phi}{R}\, e^{ik(R-r\cos\theta\sin\phi-z\cos\phi)}$$

$$\frac{\partial}{\partial r}\left(\frac{e^{ikD}}{D}\right) \rightarrow \frac{-ik\cos\theta\sin\phi}{R}\, e^{ik(R-r\cos\theta\sin\phi-z\cos\phi)} \quad . \tag{9}$$

For the far field approximation Equation (9), integration with respect to θ may be done analytically, reducing Equation (8) to an integral on the body perimeter of expressions involving ordinary Bessel functions of order zero and one. An adaptive 7-point Newton-Cotes algorithm (QNC7) is used to complete the integration in r and z. FARFLD, a subroutine in RADIAT, carries out the far field computation.

Computation of the Impedance Matrix

Pressure at any point on the vibrating surface can be found by utilizing Equation (2). If, in particular, Equation (2) is satisfied exactly at the nodes, a set of algebraic equations is formed relating nodal pressures to nodal velocities.

$$p^*_m - \sum_{\substack{\text{ISUR}\\ \text{odd}}} \sum_{j=N_1}^{N_2-1} \left\{ \frac{1}{2\pi} \int_{r_j}^{r_{j+1}} r\left[p^*_j + \frac{(p^*_{j+1} - p^*_j)}{(r_{j+1} - r_j)}(r - r_j)\right] \int_{-\pi}^{\pi} \frac{\partial}{\partial z}\left(\frac{e^{ikD}}{D}\right) d\theta dr \right\}$$

$$- \sum_{\substack{\text{ISUR}\\ \text{even}}} \sum_{j=N_1}^{N_2-1} \left\{ \frac{r}{2\pi} \int_{z_j}^{z_{j+1}} \left[p^*_j + \frac{(p^*_{j+1} - p^*_j)}{(z_{j+1} - z_j)}(z - z_j)\right] \int_{-\pi}^{\pi} \frac{\partial}{\partial r}\left(\frac{e^{ikD}}{D}\right) d\theta dz \right\} =$$

(cont)

$$= \sum_{\substack{\text{ISUR} \\ \text{odd}}} \sum_{j=N_1}^{N_2-1} \left\{ \frac{-ir}{2\pi} \int_{r_j}^{r_{j+1}} \left[u_j + \frac{(u_{j+1} - u_j)}{(r_{j+1} - r_j)} (r - r_j) \right] \int_{-\pi}^{\pi} \frac{e^{ikD}}{D} \, d\theta \, dr \right\}$$

$$+ \sum_{\substack{\text{ISUR} \\ \text{even}}} \sum_{j=N_1}^{N_2-1} \left\{ \frac{-ir}{2\pi} \int_{z_j}^{z_{j+1}} \left[u_j + \frac{(u_{j+1} - u_j)}{(z_{j+1} - z_j)} (z - z_j) \right] \int_{-\pi}^{\pi} \frac{e^{ikD}}{D} \, d\theta \, dz \right\} \tag{10}$$

where $m = 1, 2, \ldots, N$ and the distance D between node m and a point (r, θ, z) on the body is given by

$$D = \left[\left(r_m - r \cos\theta\right)^2 + (r \sin\theta)^2 + \left(z_m - z\right)^2 \right]^{1/2} .$$

Pressure and velocity at surface points between nodes are found from linear interpolation.

Equation (10) may be expressed in the form

$$A\underline{p}^* = B\underline{u}$$

where $\underline{p}^*$ and $\underline{u}$ are column vectors of the surface pressures and velocities and the matrices A and B consist of terms involving surface integrals between nodes. The impedance matrix Z is defined by

$$Z = A^{-1} B ,$$

allowing one to find the surface pressures at the nodes given any distribution of nodal velocities.

As in the case of the external pressure field computation, surface integrals must be evaluated. Integration with respect to θ is performed by an adaptive 7-point Newton-Cotes algorithm. Integration in r and z is performed from user specification by either a trapezoidal rule with functions evaluated at the nodes or an adaptive Simpson's rule algorithm. Unlike the external pressure field computation, singularities in the integrands exist at nodal points where the distance D can be zero. The trapezoidal rule option automatically breaks the interval about such a singular point into six subintervals and ignores the contribution of the subinterval containing the singularity. For the adaptive Simpson's rule, the integrand is set equal to zero at a small

distance from the singularity, in this case 10^{-6}. The legitimacy of this procedure requires that integration on a disc surrounding the singularity yields no contribution in the limit as the disc size vanishes. It can be shown that, for an isolated singularity, this is the case for the integrals encountered in this program.

In the case of the corners, the situation is more complex. Two nodes are assigned at each corner to avoid ambiguity in the definition of the normal derivative at a corner. For example, for a node j corresponding to the end node of a disc, the normal derivative is taken with respect to z while node j+1 is on a cylinder with a radial normal. This assignment is actually a limiting case of two separate nodes collapsed to the same coordinates. For the case of integrating singularities at node j (or j+1) about node j (or j+1), the integration around the small disc centered about node j (or j+1) yields the same result as for an isolated singularity. However, integration about node j (or j+1) with the singularity at node j+1 (or j) does require care, as the integrations must be considered in the limit as these nodes approach each other. To be more specific, the case when node j is on a disc surface, the normal derivative integral about a small disc d_ϵ centered about node j with the singularity at node j+1 is

$$I = \frac{-1}{2\pi}\int_{d_\epsilon} \frac{(r - r_{j-1})}{(r_j - r_{j-1})} \frac{\partial}{\partial z}\left(\frac{e^{ikD}}{D}\right) dS$$

where $D = \left\{(r\cos\theta - r_{j+1})^2 + (r\sin\theta)^2 + (z - z_{j+1})^2\right\}^{1/2}$.

To examine the limiting case of two nodes at the corner, node j+1 is displaced away from the corner a small distance Δ. Converting to a cylindrical coordinate system (α, β) centered at node j, the integral is given by

$$I = \frac{\Delta}{\pi}\int_0^\epsilon \int_0^{\pi/2} \left(1 - \frac{\alpha\cos\beta}{r_j - r_{j-1}}\right)\left(\frac{ikD - 1}{D^3}\right) e^{ikD}\, \alpha\, d\beta\, d\alpha$$

with $D = \left(\Delta^2 + \alpha^2\right)^{1/2}$ and ϵ is the radius of the small disc. Since D is small, the approximations $\sin kD = kD$ and $\cos kD = 1$ are applied, giving

$$I = \left\{ -\frac{\Delta}{2}\frac{(1 + k^2\Delta^2)}{\sqrt{\Delta^2 + \alpha^2}} - \frac{\Delta k^2}{2}\sqrt{\Delta^2 + \alpha^2} - \frac{k^2\Delta^3}{2\sqrt{\Delta^2 + \alpha^2}} \right.$$

$$+ \frac{\Delta(1 + k^2\Delta^2)}{\pi(r_j - r_{j-1})}\left[\frac{\alpha}{2}\sqrt{\alpha^2 + \Delta^2} - \frac{\Delta^2}{2}\ln\left(\alpha + \sqrt{\alpha^2 + \Delta^2}\right)\right]$$

(cont)

$$+ \frac{\Delta k^2}{\pi(r_j - r_{j-1})} \left[\frac{\alpha}{2} \sqrt{\alpha^2 + \Delta^2} + \frac{\alpha \Delta^2}{\sqrt{\alpha^2 + \Delta^2}} - \frac{3}{2} \Delta^2 \ln\left(\alpha + \sqrt{\alpha^2 + \Delta^2}\right) \right] \Bigg\} \Bigg|_0^{\epsilon} .$$

By allowing Δ to approach zero, the value of I as ϵ approaches zero is $-1/2$. This non-zero result requires that the numerical integration of this type of surface integral (which assumes no contribution from the disc d_ϵ) be adjusted by the additive factor $-1/2$. A similar result is found for the integration about node $j+1$ with the singularity at node j. The above analysis applies for a convex corner. It may be shown by similar methods that for concave corners the additive factor is $+1/2$. Finally, integration of the singular velocity integrals shows no additional contribution on the corners, and so no adjustment is made in the numerical scheme.

IV. COMPUTER CODE CHECKOUT

Verification Method

The complexity of the integral evaluations contained in the numerical solutions suggests that the legitimacy of the calculations be carefully checked out. This need is emphasized by noting the conflicting results shown in the literature. For example, the finite cylinder problem (with radius a and half-length 2a) has at least three independent solutions described in the literature [1, 3, 7]. All three of these solutions disagree quantitatively.

To provide a means for code checkout, a technique of generating exact solutions was used [1]. This method consists of placing a simple point source within the body of interest. From this source, exact normal velocity and pressure vectors may be generated. Inputting these vectors into the RADIAT code should yield a simple source field pressure distribution. The IMPED code is checked by comparing the exact pressure vector with one obtained by multiplying the impedance matrix with the exact velocity distribution.

Both RADIAT and IMPED contain user selected options to generate the simple source solutions so that correct operation of the codes may be periodically checked.

Computation Time and Error for RADIAT

The surface used for the checkout is a simple right cylinder with a length to diameter ratio of 2. Near field points are selected on the sphere located three cylinder radii from the source center. Figures 2 and 3 present near field pressures, amplitudes and phases, expressed as percent error from the known exact solution, for various azimuthal angles ϕ. Figures 2 and 3 are for 17 and 33 node grids, respectively.

The first observation is that an assignment of 17 nodes is sufficient for accuracies within 5 percent. The use of 33 nodes improves the error to less than 1 percent. In general, the use of the adaptive Simpson's rule achieves significantly higher accuracy relative to the trapezoidal rule, although this improvement costs computer time. For example, computing time per field point for Simpson's rule is greater by factors of 6 and 3 over the trapezoidal rule for the 17 and 33 node grids, respectively. It is interesting to note that the time for the Simpson's rule is essentially constant for the 17 and 33 node cases, the reason being that computing time for this technique is mainly dependent on the number of component surfaces rather than on the number of nodes. The trapezoidal rule technique always evaluates functions at the nodes and therefore doubling the number of nodes, essentially doubles the computing time.

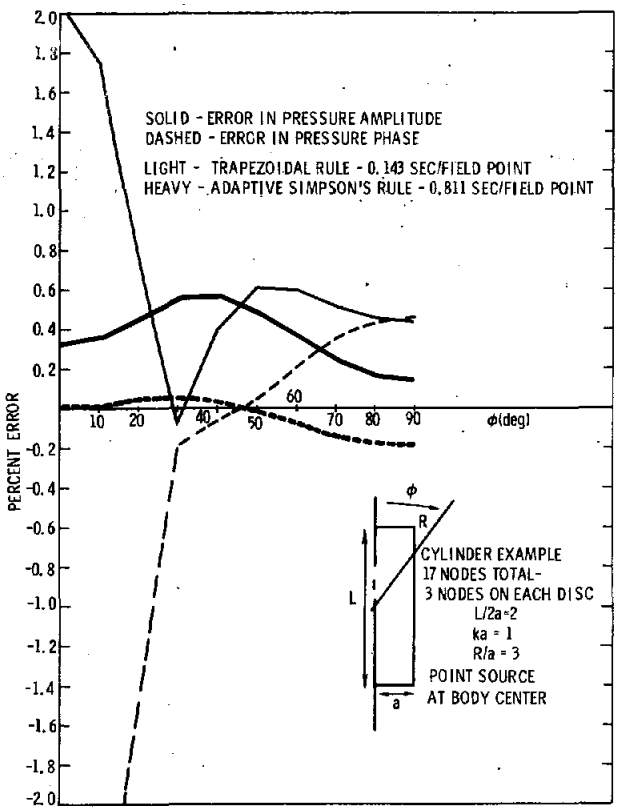

Figure 2. Near Field Pressure Calculation Accuracy, 17-Node Grid

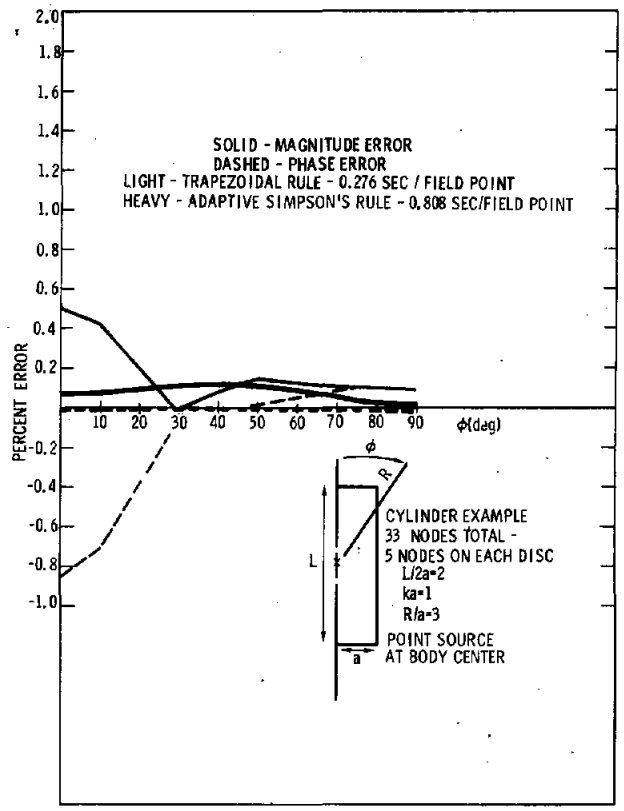

Figure 3. Near Field Pressure Calculation Accuracy, 33-Node Grid

Integration tolerance decreased below some value does not appear to improve accuracy significantly, while computing time can grow radically. Experience indicates that a tolerance of 10^{-2} is sufficient when using QNC3 and QNC7 and that a tolerance of 10^{-4} is sufficient when using the trapezoidal rule and QNC7. In any case, the user must examine the tradeoff between time and accuracy for each specific problem.

Computation Time and Error for IMPED

The simple finite cylinder of the previous section is used for checkout of the impedance matrix code IMPED. Figure 4 shows results for a 17-node grid, expressed as the percent error in pressure amplitude with point sources at two different axial positions. The Simpson's rule clearly yields the greater accuracy.

Computation time for the impedance matrix calculation is significant for both calculational schemes. For the 17-node grid, the trapezoidal rule requires 35 seconds versus 165 seconds for the adaptive Simpson's rule. As in the case for the RADIAT code, the use of either method depends on the desired tradeoff between computation time and accuracy.

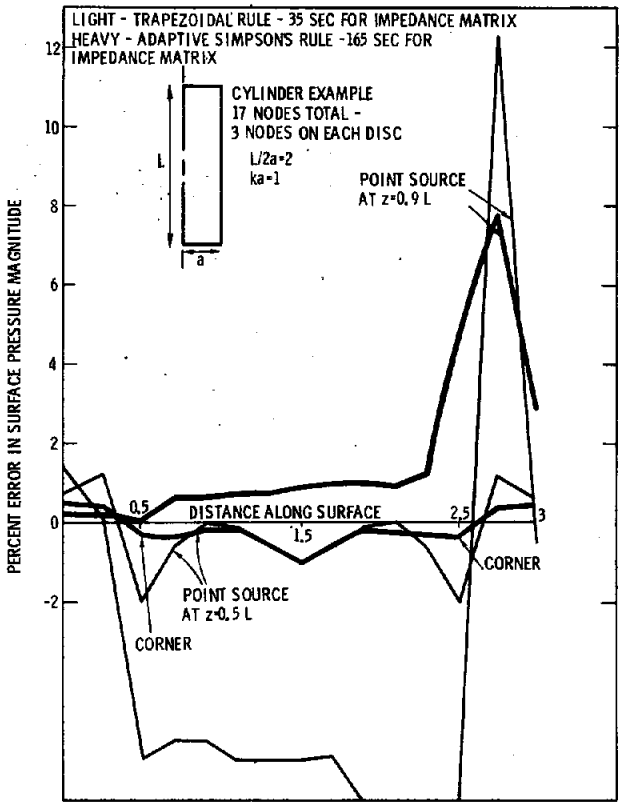

Figure 4. Surface Pressure Calculation Accuracy, 17-Node Grid

It should be noted that if the far field pressures are of interest, surface pressure errors tend to become unimportant. Figure 5 shows a comparison of far field pressure errors based on the two impedance integration options. There is apparently no sacrifice in accuracy from use of the faster trapezoidal scheme. Thus, it is concluded that unless high accuracy is desired for near field points, the adaptive Simpson's rule is not recommended.

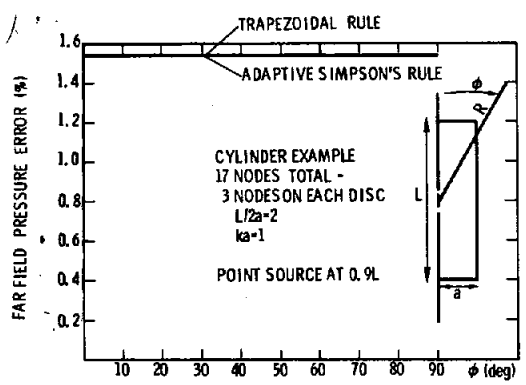

Figure 5. Far Field Pressure Based on Computed Surface Pressures and Point Source Velocity Distribution, 17-Node Grid

V. ALTERNATIVE METHOD FOR COMPUTING IMPEDANCE MATRIX

In an attempt to reduce the computation time in calculating impedance matrices, a simpler calculational method based on the spherical checkout was considered. The use of this method was not successful, but the basic idea and the shortcomings are presented as a guide to others attempting this approach.

As indicated in Figure 4, the impedance matrix quite accurately predicts the surface pressure distribution for a velocity distribution due to a point source at the center of the body. This observation is the basis for an alternative method of finding the impedance matrix. Suppose N (the number of nodes) locations are selected for point sources on the axis of the body. Since the solution for a point source is known exactly, one might attempt to find the impedance matrix from the N x N matrix equation

$$\left[\underline{p}_1 \,\vdots\, \underline{p}_2 \,\vdots\, \cdots \,\vdots\, \underline{p}_N\right] = Z\left[\underline{u}_1 \,\vdots\, \underline{u}_2 \,\vdots\, \cdots \,\vdots\, \underline{u}_N\right] \tag{11}$$

where $\underline{p}_j$ and $\underline{u}_j$ are the surface pressure and velocity distributions due to the point source at position j. Then Z may be determined by a simple matrix inversion,

$$\underline{Z} = \left[\underline{p}_1 \,\vdots\, \cdots \,\vdots\, \underline{p}_N\right]\left[\underline{u}_1 \,\vdots\, \cdots \,\vdots\, \underline{u}_N\right]^{-1} . \tag{12}$$

Such a method has been tried but appears to fail for the following reasons. The point sources cannot be located near the surface, since, as indicated in Figure 4, the impedance matrix does not predict surface pressures near the source location very well. Another possibility to locate all the point sources near the "center" of the body away from the boundary. In this case the N x N matrix of velocities becomes nearly singular giving rise to inaccuracies in the matrix inversion as required in Equation (12). What is required is to have sources for which solutions are known, closely spaced near the body center but with dissimilar velocity distributions. Solutions are known for the point source, dipole, quadrapole, etc. Thus, one could use sources having one pole up to N poles. Although not tried, it is felt that such a computation would not succeed. The higher order sources become very dependent on the azimuthal angle θ requiring a fine node structure to account for the velocity distribution. However, the more nodes selected implies the generation of even higher order sources, and an accurate velocity distribution can never be achieved.

VI. RESULTS FOR THE CYLINDER WITH RIGID END CAPS

The radiation field for the finite cylinder ($b/a = 2$) with rigid end caps and uniform radial velocity elsewhere has been calculated for moderate and low frequencies. In all the figures shown in this section, the suffixes 1 and 2 are used in describing the codes used (such as IMPED1 or RADIAT2). The suffix 1 denotes the use of the trapezoidal rule in integration, while 2 is for the adaptive Simpson's rule.

Moderate Frequency ($ka = 1$; $ka = 2$)

Figure 6 is a summary of results (normalized with respect to the pressure at $\phi = 90°$) of far and near field pressures with $ka = 1$. Also shown are the published integral method far field solutions of Schenck [1] and Copely [3] and the eigenfunction expansion results of William et al. [7] The far field calculations given here evidently agree with Schenck. The near field pressure amplitudes expressed as the ratio (P_N/P_F) of near to far field pressures differ only by a few percent from the far field results at $R/a = 3$. Figure 7 demonstrates the convergence of the near field to the far field at $\phi = 0°$ with increasing R/a. Convergence to within a few percent is rapid, but improvement beyond this level is surprisingly slow. Qualitatively similar results were obtained for other values of ϕ.

The radiation field for the relatively high frequency case of $ka = 2$ is given in Figure 8. This solution demonstrates an interference pattern, typical of radiators which produce wavelengths shorter than their characteristic length. Most of the acoustic energy in this case is directed into the main lobe centered about $\phi = 90°$. The near field pattern at $R = 3a$ is similar qualitatively, although the actual pressure magnitudes differ somewhat from the far field.

Figure 9 shows the surface pressure amplitudes for $ka = 1$ and $ka = 2$. As is the case with the far field radiation pattern, the character of the pressure distribution changes considerably with increasing frequency.

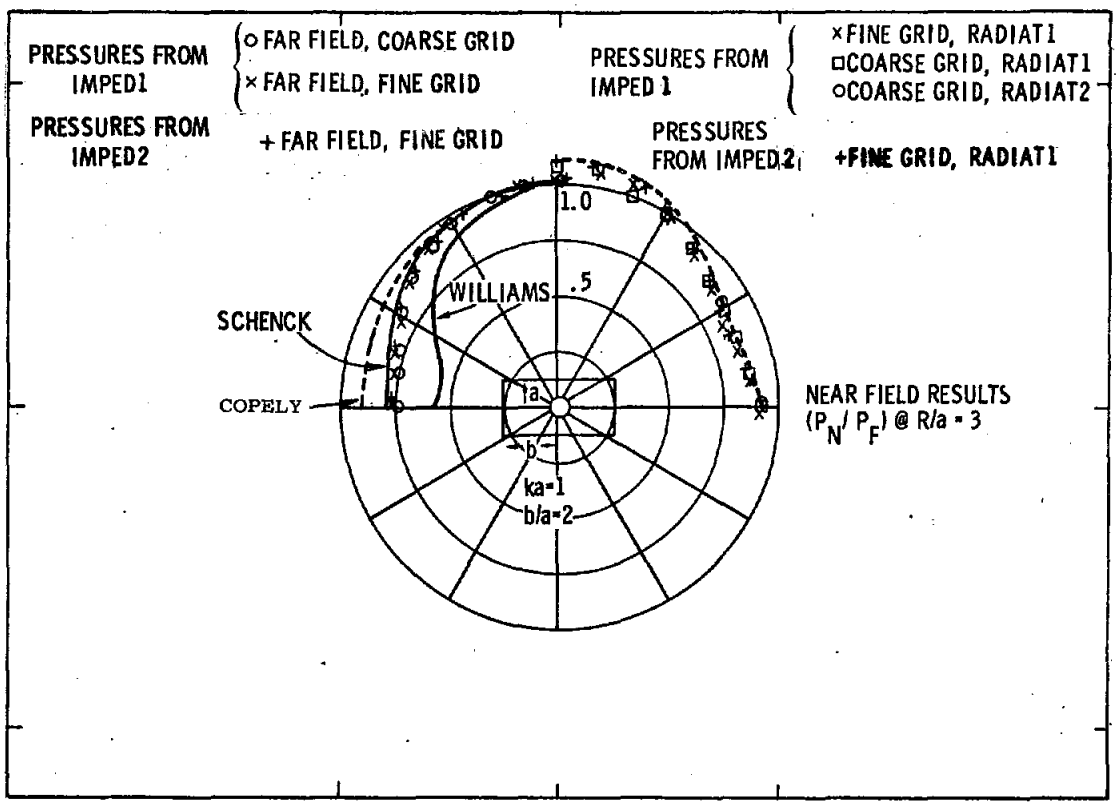

Figure 6. Near and Far Field Results, Uniform Radial Velocity on Cylinder

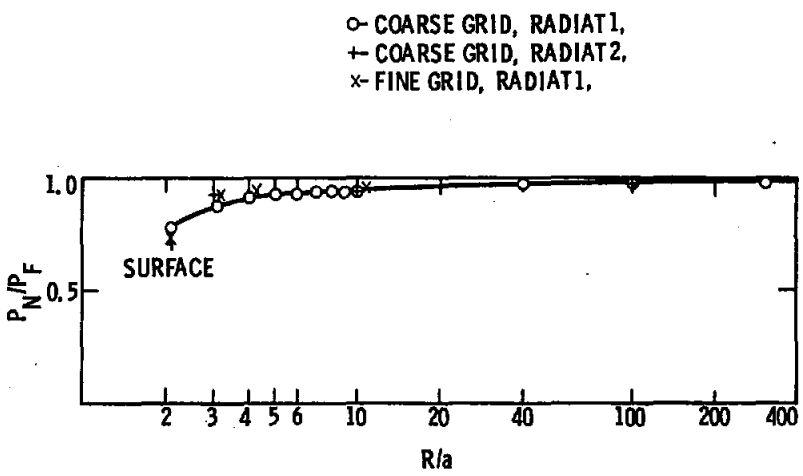

Figure 7. Convergence to Far Field, b/a = 2, ka = 1; Cylinder, Uniform Velocity Distribution, $\phi = 0°$

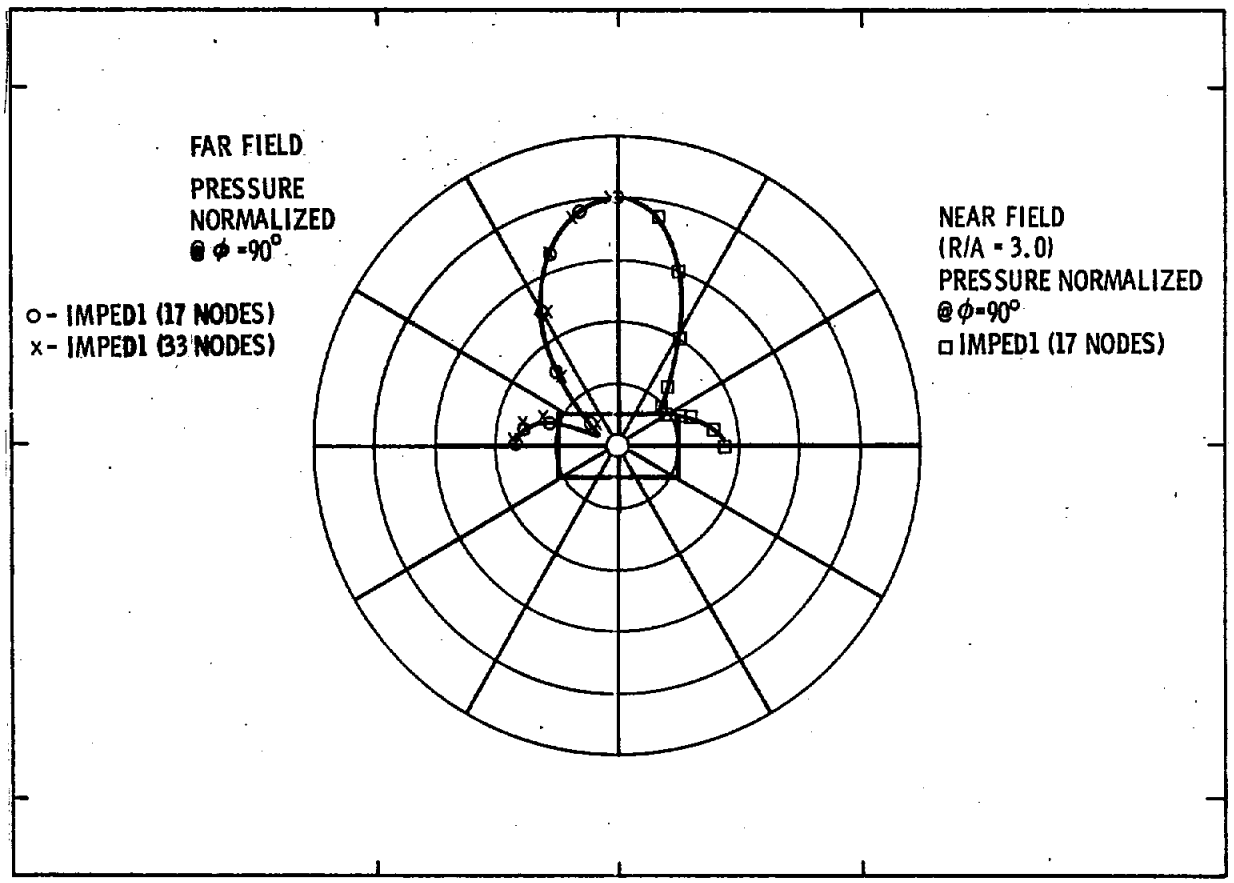

Figure 8. RADIAT1 Pressure Fields, ka = 2, b/a = 2; Uniform Radial Velocity Rigid End Caps

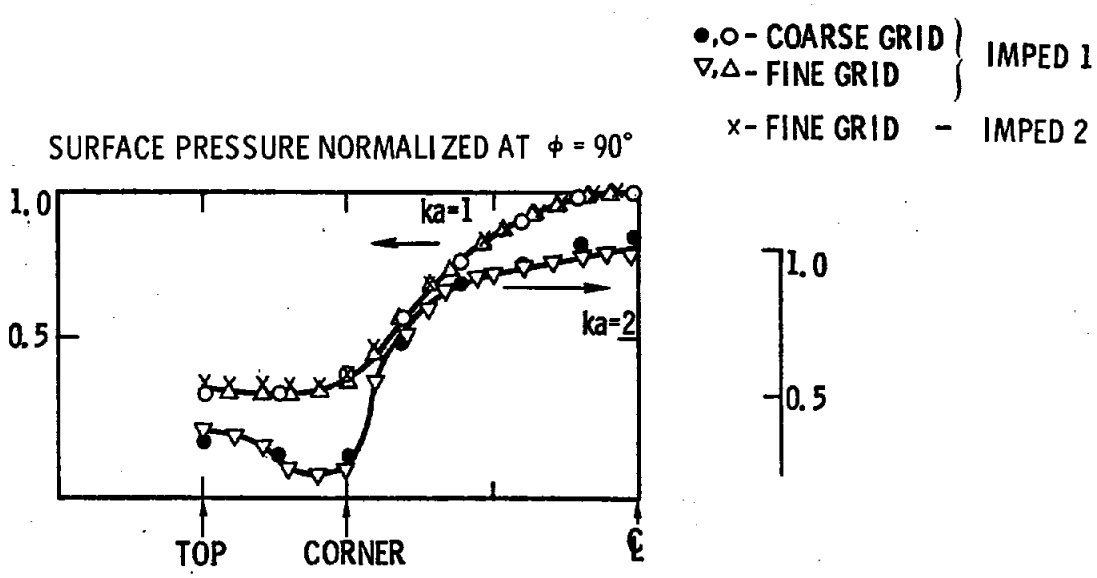

Figure 9. Uniform Velocity Pressure Distribution From IMPED Codes

Very Low Frequency (ka = 0.025)

The examination of sources which are very small relative to the radiated wavelength is of particular interest because Sandia Laboratories constructed a number of these sources. For this reason, the simple cylinder (b/a = 2) operating at ka = 0.025 has been considered.

The field pressure results are shown in Figure 10. The upper portion of the figure includes near and far field pressures for a uniform radial velocity distribution. The far field pattern is essentially spherical, a well-known characteristic of low-frequency systems. At R/a = 3, the near field shows a measurable but small deviation from the spherical radiation pattern.

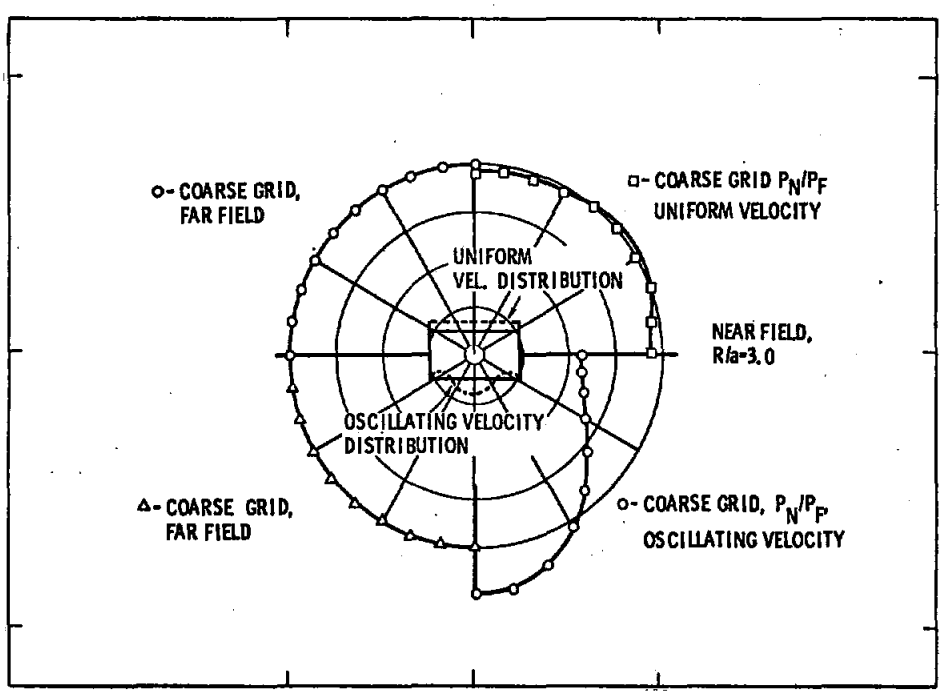

Figure 10. Low-Frequency Near and Far Field Results, (ka = 0.025); Surface Pressure Distribution From IMPED1

The influence of the surface velocity distribution on the pressure fields is examined briefly in the lower portion of Figure 10. An "oscillating" velocity distribution is used. This profile is qualitatively similar to what sometimes occurs with vibrating acoustic membranes. The influence of this motion on the near field is considerable, while the far field pattern remains spherical. It is apparent that at these low frequencies the details of the membrane motion cannot be transmitted into the far field.

Figure 11 shows the convergence of the near to far field pressures. The convergence is quite rapid for the uniform surface velocity; the oscillating profile requires considerably more distance for convergence. It is concluded that if a far field hydrophone placement is desired, some estimate of the velocity distribution is required. For experiments conducted at Sandia with a similar geometry, a hydrophone location at 15 radii has been used. The preliminary results of this study indicate that this placement should be well into the far field even for non-uniform velocity distributions.

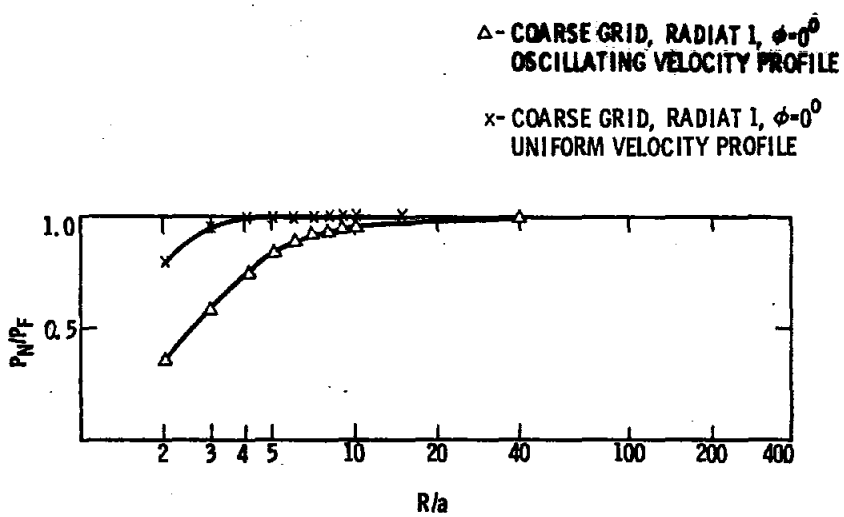

Figure 11. Convergence to Far Field; b/a = 2, ka = 0.025

VII. SUMMARY AND CONCLUSIONS

Two computer codes are presented for determining the near field, far field, and surface pressure distributions on vibrating cylindrical bodies. The codes have been tested through the generation of exact, simple source solutions. The numerical results generally deviate from the exact solution by less than 5 percent; improvement on that percent is possible with additional computer time.

Calculation of near and far field pressures, given the body surface pressure distribution, requires little computer time (generally less than 1 second per field point). However, the body surface pressure distribution is costly to generate. This cost is partially alleviated by constructing impedance matrices in a separate code. With the separate code, impedance matrices for a given geometry may be generated once and for all for the repeated use in the radiation code or in structural programs.

The codes applied to the simple cylinder with rigid end caps and uniform, moderate frequency, radial velocity elsewhere produced far field pressures in agreement with Schenck's results [1]. The very low frequency vibration of a similar cylinder indicates that the far field pattern is, as expected, spherical. The convergence to this spherical field with radial distance from the source is rapid, occurring within a few source radii. The specific rate of convergence was found to be affected by the nature of the velocity distribution on the cylinder.

The current codes apply only for connected cylinder disc combinations with axially symmetric velocity distributions. The generalization to other geometrics is possible but would require new, more complicated coding. In view of Sandia's interest in cylindrical sources, the more general coding was not considered appropriate for this report.

REFERENCES

[1] Schenck, H. A., "Improved Integral Formulation for Acoustic Radiation Problems," J. Acoust. Soc. Am., 44, 1968, pp 41-58.

[2] Chertock, G., "Sound Radiation from Vibrating Surfaces," J. Acoust. Soc. Am., 36, 1964, pp 1305-1313.

[3] Copley, L. G., "Integral Equation Method for Radiation from Vibrating Bodies," J. Acoust. Soc. Am., 41, 1967, pp 807-816.

[4] Iau, H. K. and Martenson, A. J., "A Numerical Technique for Solving Acoustic Radiation Problems," Rpt. No. N70-35075, G. F. Mechanical Engineering Lab, Schenectady, New York, October 1969.

[5] Smith, R. R., Hunt, J. T., and Barach, D., "Finite Element Analysis of Acoustically Radiating Structures with Applications to Sonar Transducers," J. Acoust. Soc. Am., 54, 1973, pp 1277-1288.

[6] Bailey, C. B. and Jones, R. E., "Brief Instructions for Using the Sandia Numerical Mathematical Subroutine Library on the CDC 6600," SLA-74-0095, Sandia Laboratories, Albuquerque, NM, April 1974.

[7] Williams, W., Parke, N. G., Moran, D. A., and Sherman, C. H., "Acoustic Radiation from a Finite Cylinder," J. Acoust. Soc. Am., 36, 1964, pp 2316-2322.

APPENDIX A

INPUT/OUTPUT INFORMATION FOR RADIAT AND IMPED

Program RADIAT

Input

Card	Parameter	Format	Columns	Description
1	M	I2	1-2	M=0 Read impedance matrix, read velocities M=1 Read impedance matrix, point source velocities M=2 Point source pressures and velocities
1	INTGR	I2	3-4	INTGR=1 Trapezoidal rule integration INTGR=2 Adaptive Simpson's rule integration
2	N	I2	1-2	Number of nodes
2	NCØR	I2	3-4	Number of corners
2	(ICØR(I),I=1, NCØR)	5I2	5-14	First node at each corner
3	ZO	F10.0	1-10	z coordinate value for Node 1
3	(DRZ(I),I=1, NSUR)	5F10.0	11-60	Change in z or r coordinate for each component
4	FK	F10.0	1-10	Wave number
if M=0 or 1 5	((ZI(I,J),ZR(I,J), J=1,N),I=1,N)	6E13.6		Imaginary, real part of impedance matrix
if M=0 6	NØDE	I4	1-4	Node at which velocity is to be given
6	U1	F8.2	5-12	Real part of velocity
6	U2	F8.2	13-20	Imaginary part of velocity
if M=1 6 if M=2 5	ZPNT	F10.0	1-10	z coordinate of point source location

(cont)

Program RADIAT (cont)

Card	Parameter	Format	Columns	Description
if M=0 or 1 7 if M=2 6	RF	F10.0	1-10	Radial distance to field point
if M=0 or 1 7 if M=2 6	PHI	F10.0	11-20	Angle (degrees) to field point

Note: Card 6 is read until NØDE=0 is encountered.
RF, PHI cards can be stacked, end-of-file causes program stop.

Sample Input

```
M=2
INTGR=1
N=17
NCØR=2
(ICØR(I),I=1,NCØR)=3,14
ZO=-1.
(DRZ(I),I=1,NSUR)=+.5,+2.,-.5
FK=2.
ZPNT=0.
RF=3.
PHI=0.,10,20,30,40,50,60,70,80,90
```

Program RADIAT (cont)

Sample Output

ACCOUSTIC RADIATION CALCULATION

OPERATING CONDITIONS - K= 2.0, OPTION = 2, INTEGRATION = 1

POINT SOURCE AT R=0,Z= 0.

NODE NO.	RADIAL	AXIAL	SPECIFIED VELOCITY REAL	SPECIFIED VELOCITY IMAG	WALL PRESSURE REAL	WALL PRESSURE IMAG	WALL PRESSURE AMPLITUDE
1	0.00	-1.00	1.00	1.24	.64836E+00	.29673E+00	.71304E+00
2	.25	-1.00	.88	1.21	.61011E+00	.32602E+00	.69175E+00
3	.50	-1.00	.58	1.11	.50176E+00	.39367E+00	.63776E+00
4	.50	-1.00	.29	.55	.50176E+00	.39367E+00	.63776E+00
5	.50	-.80	.63	.65	.71840E+00	.23488E+00	.75582E+00
6	.50	-.60	1.18	.74	.91292E+00	-.79849E-02	.91295E+00
7	.50	-.40	2.05	.80	.10670E+01	-.31861E+00	.11136E+01
8	.50	-.20	3.25	.84	.11659E+01	-.62754E+00	.13241E+01
9	.50	0.00	3.94	.86	.12000E+01	-.77051E+00	.14261E+01
10	.50	.20	3.25	.84	.11659E+01	-.62754E+00	.13241E+01
11	.50	.40	2.05	.80	.10670E+01	-.31861E+00	.11136E+01
12	.50	.60	1.18	.74	.91292E+00	-.79849E-02	.91295E+00
13	.50	.80	.63	.65	.71840E+00	.23488E+00	.75582E+00
14	.50	1.00	.29	.55	.50176E+00	.39367E+00	.63776E+00
15	.50	1.00	.58	1.11	.50176E+00	.39367E+00	.63776E+00
16	.25	1.00	.88	1.21	.61011E+00	.32602E+00	.69175E+00
17	0.00	1.00	1.00	1.24	.64836E+00	.29673E+00	.71304E+00

FIELD PRESSURE VALUES-

RADIAL	ANGLE	FAR FIELD REAL	FAR FIELD IMAG	FAR FIELD AMPLITUDE	NEAR FIELD REAL	NEAR FIELD IMAG	NEAR FIELD AMPLITUDE
1.50	0.00	.658408E-01	.466711E+00	.471332E+00	.640776E+00	.993368E+00	.987693E+00
1.50	10.00	.658564E-01	.466846E+00	.471468E+00	.705055E+00	.995439E+00	.990588E+00
1.50	20.00	.659039E-01	.467218E+00	.471843E+00	.857861E+00	.100233E+01	.999707E+00
1.50	30.00	.659843E-01	.467734E+00	.472366E+00	.997818E+00	.100732E+01	.100713E+01
1.50	40.00	.660980E-01	.468283E+00	.472925E+00	.100491E+01	.100125E+01	.100133E+01
1.50	50.00	.662359E-01	.468737E+00	.473394E+00	.101096E+01	.997726E+00	.997987E+00
1.50	60.00	.663818E-01	.469044E+00	.473718E+00	.102581E+01	.996907E+00	.997482E+00
1.50	70.00	.665173E-01	.469203E+00	.473894E+00	.103836E+01	.997029E+00	.997860E+00
1.50	80.00	.666101E-01	.469260E+00	.473964E+00	.104606E+01	.997336E+00	.998323E+00
1.50	90.00	.666418E-01	.469272E+00	.473980E+00	.104863E+01	.997479E+00	.998516E+00

Program IMPED

Input

Card	Parameter	Format	Columns	Description
1	IPRNT	I2	1-2	≥ 1 Print impedance matrix < 1 Don't print
1	IPNCH	I2	3-4	≥ 1 Punch impedance matrix ((ZI(I, J), ZR(I=J), J=1, N), I=1, N) under 6E13.6 < 1 Don't punch
1	INTGR	I2	5-6	INTGR=1 Trapezoidal rule integration INTGR=2 Adaptive Simpson's rule integration
2	N	See program RADIAT		
2	NCØR			
2	(ICØR(I), I=1, NCØR)			
3	ZO			
3	(DRZ(I), I=1, NSUR)			
4	FK			
5	ZPNT			

Note: ZPNT cards can be stacked, end-of-file causes program stop.

Sample Input

```
IPRNT=0
IPNCH=0
INTGR=1
N=17
NCØR=2
(ICØR(I),I=1,NCØR)=3,14
ZO=-1.
(DRZ(I),I=1,NSUR)=+.5,+2.,-.5
FK=2.
ZPNT=0.,.4,.8
```

Program IMPED (cont)

Sample Output

COUSTIC IMPEDANCE CALCULATION

K= 2.0 INTEGRATION=1

POINT SOURCE AT R=0,Z= 0.

NODE	RADIAL	AXIAL	COMPUTED SURFACE PRESSURE/POINT SOURCE PRESSURE
1	0.00	-1.00	.100663E+01
2	.25	-1.00	.101160E+01
3	.50	-1.00	.980026E+00
4	.50	-1.00	.980026E+00
5	.50	-.80	.994146E+00
6	.50	-.60	.100053E+01
7	.50	-.40	.998866E+00
8	.50	-.20	.993909E+00
9	.50	0.00	.990232E+00
10	.50	.20	.993909E+00
11	.50	.40	.998866E+00
12	.50	.60	.100053E+01
13	.50	.80	.994146E+00
14	.50	1.00	.980026E+00
15	.50	1.00	.980026E+00
16	.25	1.00	.101160E+01
17	0.00	1.00	.100663E+01

POINT SOURCE AT R=0,Z= .400000E+00

NODE	RADIAL	AXIAL	COMPUTED SURFACE PRESSURE/POINT SOURCE PRESSURE
1	0.00	-1.00	.101755E+01
2	.25	-1.00	.101418E+01
3	.50	-1.00	.979982E+00
4	.50	-1.00	.979982E+00
5	.50	-.80	.996081E+00
6	.50	-.60	.100257E+01
7	.50	-.40	.100216E+01
8	.50	-.20	.100220E+01
9	.50	0.00	.999683E+00
10	.50	.20	.992816E+00
11	.50	.40	.986497E+00
12	.50	.60	.985991E+00
13	.50	.80	.981961E+00
14	.50	1.00	.973975E+00
15	.50	1.00	.973975E+00
16	.25	1.00	.101317E+01
17	0.00	1.00	.992094E+00

POINT SOURCE AT R=0,Z= .800000E+00

NODE	RADIAL	AXIAL	COMPUTED SURFACE PRESSURE/POINT SOURCE PRESSURE
1	0.00	-1.00	.101354E+01
2	.25	-1.00	.100102E+01
3	.50	-1.00	.940638E+00
4	.50	-1.00	.940638E+00
5	.50	-.80	.945818E+00
6	.50	-.60	.945031E+00
7	.50	-.40	.940403E+00
8	.50	-.20	.940464E+00
9	.50	0.00	.941265E+00
10	.50	.20	.938691E+00
11	.50	.40	.928812E+00
12	.50	.60	.907413E+00
13	.50	.80	.884670E+00
14	.50	1.00	.901132E+00
15	.50	1.00	.901132E+00
16	.25	1.00	.112207E+01
17	0.00	1.00	.995425E+00

Program RADIAT (or IMPED) - Control Cards

```
Jobcard, 100-K CM required
Account card
ATTACH,ØLDPL,RADIAT(OR IMPED),CY=1.
UPDATE,F.
FTN,I=CØMPILE.
CØLLECT,LGØ,FTNLIB,FXMATH.
LGØ.
7/8/9
7/8/9
Data
6/7/8/9
```

DISTRIBUTION:

1500	R. L. Peurifoy
1540	T. B. Lane
1541	S. W. Key
1543	H. C. Hardee
1544	R. T. Othmer
1544	W. N. Sullivan (5)
4700	D. B. Shuster
4730	R. G. Clem
4731	W. F. Roherty
4734	V. L. Dugan
4734	J. F. Banas (5)
5700	J. H. Scott
5710	G. E. Brandvold
5712	R. H. Braasch
5712	E. G. Kadlec
9414	V. M. Brewster
9414	M. T. Mattison
8266	E. A. Aas (2)
3141	L. S. Ostrander (5)
3151	W. L. Garner (3)
	For ERDA/TIC (Unlimited Release)